Available online at www.sciencedirect.com
SCIENCE DIRECT®
Bioorganic & Medicinal Chemistry 14 (2006) 181–189
Bioorganic & Medicinal Chemistry

Crystallographic studies on two bioisosteric analogues, *N*-acetyl-β-D-glucopyranosylamine and *N*-trifluoroacetyl-β-D-glucopyranosylamine, potent inhibitors of muscle glycogen phosphorylase

Eleni Anagnostou,[a,†] Magda N. Kosmopoulou,[a] Evangelia D. Chrysina,[a] Demetres D. Leonidas,[a] Theodoros Hadjiloi,[a] Costantinos Tiraidis,[a] Spyros E. Zographos,[a] Zoltán Györgydeák,[c] László Somsák,[c] Tibor Docsa,[d] Pál Gergely,[d] Fragiskos N. Kolisis[e] and Nikos G. Oikonomakos[a,b,*]

[a]*Institute of Organic and Pharmaceutical Chemistry, The National Hellenic Research Foundation, 48, Vas. Constantinou Ave. 116 35 Athens, Greece*
[b]*Institute of Biological Research and Biotechnology, The National Hellenic Research Foundation, 48, Vas. Constantinou Ave. 116 35 Athens, Greece*
[c]*Department of Organic Chemistry, Research Centre for Molecular Medicine, University of Debrecen, Hungary*
[d]*Department of Medical Chemistry, Research Centre for Molecular Medicine, University of Debrecen, Hungary*
[e]*Biotechnology Laboratory, School of Chemical Engineering, The National Technical University of Athens, Greece*

Received 30 March 2005; accepted 2 August 2005
Available online 4 October 2005

Abstract—Structure-based inhibitor design has led to the discovery of a number of potent inhibitors of glycogen phosphorylase b (GPb), *N*-acyl derivatives of β-D-glucopyranosylamine, that bind at the catalytic site of the enzyme. The first good inhibitor in this class of compounds, *N*-acetyl-β-D-glucopyranosylamine (NAG) (K_i = 32 μM), has been previously characterized by biochemical, biological and crystallographic experiments at 2.3 Å resolution. Bioisosteric replacement of the acetyl group by trifluoroacetyl group resulted in an inhibitor, *N*-trifluoroacetyl-β-D-glucopyranosylamine (NFAG), with a K_i = 75 μM. To elucidate the structural basis of its reduced potency, we determined the ligand structure in complex with GPb at 1.8 Å resolution. To compare the binding mode of *N*-trifluoroacetyl derivative with that of the lead molecule, we also determined the structure of GPb–NAG complex at a higher resolution (1.9 Å). NFAG can be accommodated in the catalytic site of T-state GPb at approximately the same position as that of NAG and stabilize the T-state conformation of the 280s loop by making several favourable contacts to Asn284 of this loop. The difference observed in the K_i values of the two analogues can be interpreted in terms of subtle conformational changes of protein residues and shifts of water molecules in the vicinity of the catalytic site, variations in van der Waals interaction, and desolvation effects.

1. Introduction

Efforts towards improving glycaemic control in type 2 diabetes mellitus have been lately directed towards developing inhibitors of glycogen phosphorylase (GP), an enzyme proposed to be exploited as a therapeutic molecular target.[1–5] Several regulatory binding sites of GP have been identified and are currently under investigation for the design and synthesis of potent inhibitors of the enzyme.[3,6–13] More specifically, the catalytic site has been probed with glucose analogue inhibitors, designed on the basis of information derived from the crystal structure of the inactive T-state GPb–α-D-glucose complex.[14–26] A common feature of these compounds is that upon binding at the catalytic site, they promote the (less active) T-state conformation of the enzyme

Keywords: Type 2 diabetes; Glycogen phosphorylase; *N*-acetyl-β-D-glucopyranosylamine; *N*-trifluoroacetyl-β-D-glucopyranosylamine; Bioisosteric inhibition; X-ray crystallography.
* Corresponding author. Tel.: +30 210 7273761; fax: +30 210 7273831; e-mail: ngo@eie.gr
† Present address: Institute of Marine and Coastal Science, RUTGERS, New Brunswick, NJ, USA.

0968-0896/$ - see front matter © 2005 Elsevier Ltd. All rights reserved.
doi:10.1016/j.bmc.2005.08.010

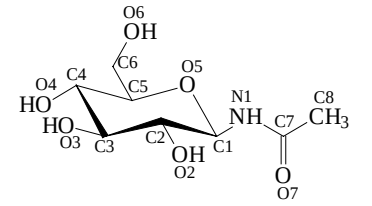

NAG

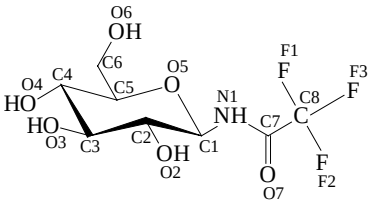

NFAG

Scheme 1. Chemical structures of *N*-acetyl-β-D-glucopyranosylamine (NAG) and *N*-trifluoroacetyl-β-D-glucopyranosylamine (NFAG), showing the numbering system used.

through stabilization of the closed position of 280s loop (residues 282–287), which blocks access of the substrate to the catalytic site.

One of the early successes was the design and synthesis of *N*-acetyl-β-D-glucopyranosylamine (NAG, Scheme 1), which exhibited a potency to inhibit GP activity (K_i = 32 μM), approximately 50 times better than that of α-D-glucose (K_i = 1.7 mM).[17] Extensive physiological studies showed that NAG was indeed an effective inhibitor of liver GPa in rat hepatocytes and that it was able to enhance the dephosphorylation (inactivation) of GPa,[27–29] indicating a potential hypoglycaemic action in the treatment of type 2 diabetes. Information available from the crystal structure of T-state GPb–NAG–IMP complex at 2.3 Å resolution has shown that NAG fits neatly into the so-called β-pocket, a side channel from the catalytic site, lined by both polar and nonpolar groups, but with no access to the bulk solvent,[14] and binding is stabilized through a strong hydrogen bond formed between the amide nitrogen and the main chain carbonyl O of His377.[17] Following crystallographic analysis of the NAG complex, modelling of other compounds was performed, torsion angles were adjusted to allow favourable interactions with the protein, and a large number of derivatives were synthesized with the objective of identifying more potent inhibitors.[18] The compounds synthesized differed only in their substituent atoms at the β-configuration at the C1 position of the glucopyranose ring, but none of the NAG analogues studied resulted in improved K_i values compared with the lead molecule.[18] In a recent study,[24] it has been demonstrated that a substituent with a longer chain and larger, more hydrophobic group facilitates stronger binding (K_i = 3.5 μM for *N*-(2-naphthylacryloyl)-β-D-glucopyranosylamine). A better understanding of the mechanism of inhibition of GP through identification of the structural determinants contributing to inhibitor interactions at the β-pocket should aid in the design of improved inhibitors against GP.

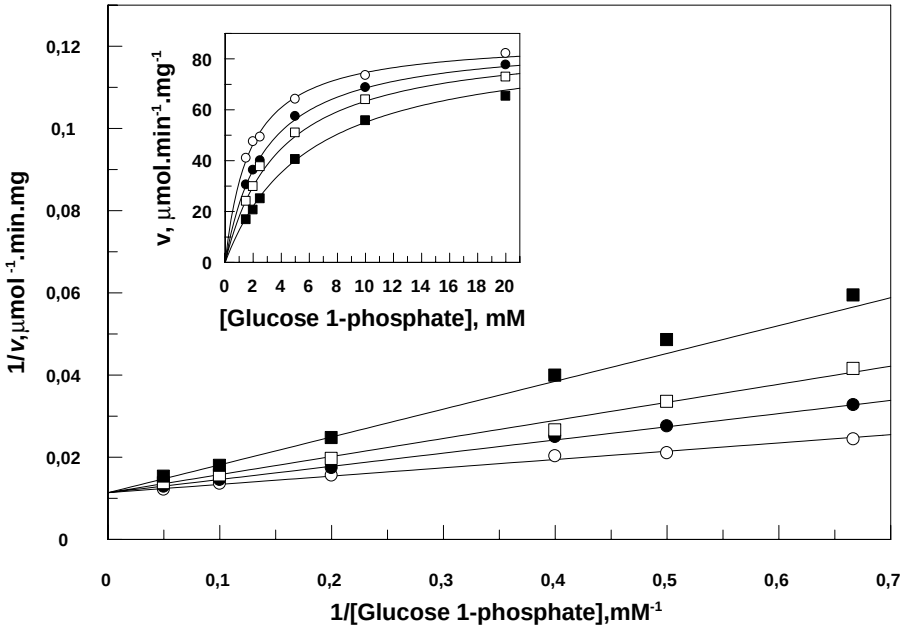

Figure 1. Kinetics of NFAG inhibition of GPb with respect to Glc-1-P (3, 4, 6, 10, 20 mM) in the direction of the glycogen synthesis (30 °C, pH 6.8). Double reciprocal plots of initial reaction velocity versus [Glc-1-P] at constant concentrations of AMP (1 mM) and glycogen (1%) and various concentrations of NFAG. Inhibitor concentrations (mM) were as follows: 0 (○), 0.044 (●), 0.089 (□) and 0.178 mM (■). Best-fit lines were computer generated according to the equation for competitive inhibition[43] by fitting all of the data at once. The kinetic parameters determined by this method are as follows: K_m = 1.8 ± 0.1 mM, k = 87.9 ± 0.9 U/mg and K_i = 0.075 ± 0.004 mM. Inset (top left): Fit of the calculated lines to the initial rate measurements.

We report here on the kinetic and crystallographic experiments of *N*-trifluoroacetyl-β-D-glucopyranosylamine (NFAG) with GPb. The change from $-CH_3$ in NAG to a $-CF_3$ in NFAG was found to result in a decrease in inhibitory action (K_i = 75 μM) towards GPb. To obtain information on the mechanism of NFAG inhibition of the enzyme, we determined the crystal structure of GPb complexed with NFAG at 1.8 Å resolution. The crystallographic results show that on binding of NFAG to the enzyme there were subtle changes in the vicinity of the catalytic site that can provide a rationale for the kinetic properties of the inhibitor. A new crystallographic data set of GPb–NAG complex was also collected at 1.9 Å resolution for a more accurate comparison with the GPb–NFAG complex.

2. Results

We have shown previously that NAG is an effective competitive inhibitor of GPb, with a K_i value of 32 (±1) μM.[30] The inhibitory efficiency of NFAG was also tested with GPb (Fig. 1). The compound displayed competitive inhibition with respect to the substrate Glc-1-P, at constant concentrations of glycogen (1% w/v) and AMP (1 mM). The inhibition constant of NFAG for muscle GPb, assayed into the direction of glycogen synthesis, is $K_i = 75 \pm 4$ μM, approximately 2.3 times larger than NAG, which points to a difference in the binding energy between NFAG and NAG of about 0.51 kcal/mol (in a previous report,[20] a K_i value of 710 μM was erroneously given for the NFAG inhibition of GPb). To elucidate the structural basis of this difference in affinity, we have determined the crystal structures of GPb in complex with both NAG and NFAG.

A summary of the crystallographic data processing and refinement statistics is given in Table 1. A schematic representation of the native T-state structure of GPb with the distinct catalytic, allosteric effector and the new allosteric inhibitor binding sites is shown in Figure 2. Electron density maps defined the position of each inhibitor within the catalytic site (Fig. 3A and B), consistent with the kinetic results. Furthermore, there was clear additional density contributed by the fluorine atoms. We describe briefly the GPb/NAG interactions and in more detail the GPb/NFAG interactions at the catalytic site.

Table 1. Diffraction data and refinement statistics for GPb–NAG and GPb–NFAG complexes

	GPb–NAG	GPb–NFAG
Experiment	10 mM NAG	100 mM NFAG
Space group	$P4_32_12$	$P4_32_12$
No. of images (°)	74 (0.7)[a]	90 (0.5)[a]
Unit cell dimensions (Å)	$a = b = 128.6$, $c = 116.1$	$a = b = 128.8$, $c = 116.2$
Resolution range (Å)	29.36–1.90	28.07–1.80
No. of observations	507267	568131
No. of unique reflections	68661	89632
$\langle I/\sigma(I)\rangle$ (outermost shell)[b]	6.6 (2.4)	11.9 (1.9)
Completeness (outermost shell) (%)	89.2 (89.5)	99.0 (97.5)
R_m (outermost shell)[c]	0.097 (0.445)	0.041 (0.420)
Outermost shell (Å)	1.93–1.90	1.83–1.80
Multiplicity (outermost shell)	4.1 (3.6)	3.7 (3.6)
Refinement (resolution) (Å)	29.36–1.90	28.07–1.80
No. of reflections used (free)	65135 (3495)	85072 (4511)
Residues included	(12–251), (261–341), (324–837)	(12–252), (261–314), (324–837)
No. of protein atoms	6585	6596
No. of water molecules	356	402
No. of ligand atoms	15 (PLP), 15 (NAG)	15 (PLP), 18 (NFAG)
Final R (R_{free})[d] (%)	18.8 (21.1)	19.0 (21.5)
R (R_{free}) (outermost shell) (%)	25.6 (27.3)	27.6 (29.9)
Outermost shell in refinement (Å)	2.02–1.90	1.91–1.80
r.m.s.d. in bond lengths (Å)	0.006	0.006
r.m.s.d. in bond angles (°)	1.3	1.3
r.m.s.d. in dihedrals (°)	22.1	22.0
r.m.s.d. in impropers (°)	0.93	0.77
Average B (Å^2) for residues	(12–251), (261–314), (324–837)	(12–252), (261–314), (324–837)
Overall	32.4	32.2
CA,C,N,O	30.3	30.1
Side chain	34.4	34.3
Average B (Å^b) for ligands	19.9 (PLP), 20.2 (NAG)	19.8 (PLP), 21.8 (NFAG)
Average B (Å^b) for water molecules	41.6	43.0

[a] 0.5/0.7 is the rotation range per image.

[b] $\sigma(I)$ is the standard deviation of I.

[c] $R_{merge} = \sum_i \sum_h |\langle I_h\rangle - I_{ih}| / \sum_i \sum_h I_{ih}$, where $\langle I_h\rangle$ and I_{ih} are the mean and ith measurement of intensity for reflection h, respectively.

[d] Crystallographic $R = \sum ||F_o| - |F_c|| / \sum |F_o|$, where $|F_o|$ and $|F_c|$ are the observed and calculated structure factor amplitudes, respectively. R_{free} is the corresponding R value for a randomly chosen 5% of the reflections that were not included in the refinement.

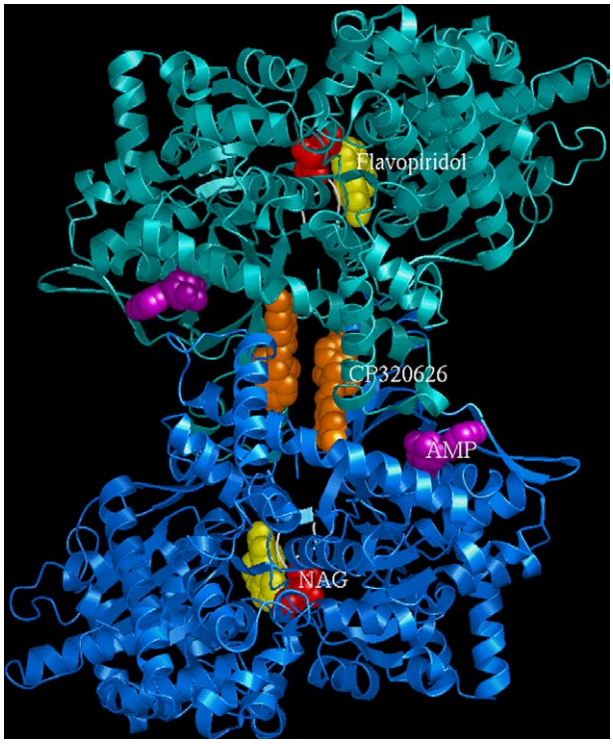

Figure 2. A schematic diagram of the T-state GPb dimeric molecule, viewed down the molecular dyad, showing the positions for the catalytic, allosteric, inhibitor and new allosteric binding sites. The catalytic site is buried at the centre of the subunit accessible to the bulk solvent through a 15 Å long channel. NAG (shown in red) binds at this site and promotes the less active T state through stabilization of the closed position of the 280s loop (shown in white). The allosteric site, which binds the activator AMP (shown in magenta), is situated at the subunit-subunit interface some 30 Å from the catalytic site. The inhibitor site, which binds purine compounds, such as caffeine, and flavopiridol (shown in yellow) is situated at the entrance to the catalytic site tunnel, formed by two hydrophobic residues of Phe285 and Tyr613. The new allosteric or indole binding site, located inside the central cavity formed on association of the two subunits, binds the CP320626 molecule (shown in orange).

2.1. NAG binding

The mode of binding and the interactions that NAG makes with GPb are similar to those that have been described previously in the 2.3 Å resolution structure of the GPb–NAG–IMP complex.[17] The glucopyranose moiety makes one less hydrogen bond with the protein than in the α-D-glucose complex due to the absence of –OH at 1 position since NAG is a β-D-glucose analogue. However, there is a hydrogen bond between N1 of NAG and carbonyl O of His377, an interaction that is conserved in all β-D-glucopyranosylamine and spirohydantoin analogues of β-D-glucopyranose studied so far.[6,18,23,25,26] There are, in total, 15 hydrogen bonds and 61 van der Waals interactions (6 nonpolar/nonpolar, 10 polar/polar and 45 nonpolar/polar) (Table 2) in the GPb–NAG complex. The hydrogen bonds formed between the ligand and the protein are shown in Figure 4A. Three water molecules, not identified in the previous structural study, were found to be located in the vicinity of the catalytic site, Wat106, Wat110 and Wat314. Wat106 is hydrogen bonded to Glu88 OE1, Asn282 O, and makes a water-mediated link to Asn284 N and ligand O7 atom (through Wat355). Wat110 is hydrogen bonded to His341 NE2 of the β-pocket, Asp339 OD1 and Ala383 of O through water Wat109. Wat314 is hydrogen bonded to Asp283 OD2, Lys574 NZ, Tyr573 OH and another water molecule (Wat104) which itself interacts directly with Gly135 N and Asp283 OD1 and indirectly with Arg569 N, PLP O2P, Tyr573 OH and Lys574 NZ, through an extensive water-mediated hydrogen bonding network. The contacts that NAG makes with Asn284 (1 hydrogen bond and 8 van der Waals contacts) are maintained in both the 1.9 and 2.3 Å resolution structures and promote a closed geometry of the 280s loop (residues 282–287) occurring in the T-state GPb.

2.2. NFAG binding

The ligand binds at the catalytic site of the enzyme in the same mode as the lead molecule, and exploits a total of 15 hydrogen bonds and 75 van der Waals interactions (4 nonpolar-nonpolar, 19 polar-polar and 52 nonpolar/polar) (Table 3). The hydrogen bond of the amide nitrogen (N1) with His377 O is retained. There are two additional polar contacts in comparison to the GPb–NAG complex; atoms F2 and F3 make rather short contacts (3.2 Å) to Wat315. The water-mediated hydrogen bonds between NFAG and GPb are also maintained, with the exception of the hydrogen bonds between O2 of NFAG and Lys574 NZ, Asn284 ND2, Tyr573 OH, Asp383 OD2 and Wat99 through Wat319, and F2, F3, O7 polar contacts to Wat314 through Wat315. The fluorine atoms of NFAG are involved in 21 van der Waals interactions with the GPb molecule. However, the carbon C8 of the

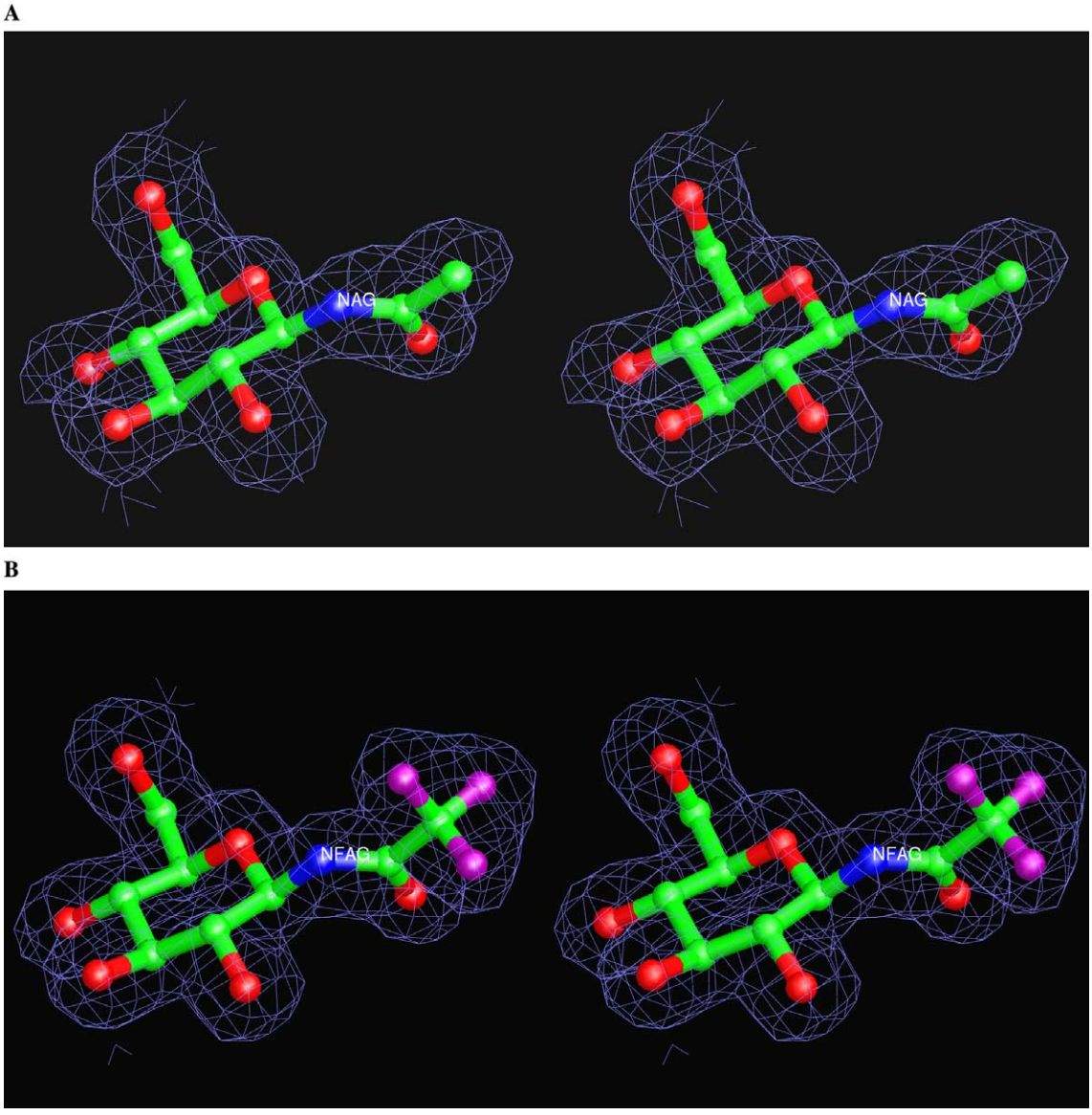

Figure 3. $2F_o-F_c$ electron density maps of the refined NAG (A) and NFAG (B) structures bound at the catalytic site of GPb. The maps are contoured at the 1.0 σ level.

inhibitor NFAG forms four less van der Waals interactions with the protein; there is one interaction with Asn284 OD1 and one with a water molecule (Wat315), while in the GPb–NAG complex carbon C8 interacts additionally to another water molecule and Asn284 CG, ND2 as well as with Asp339 OD1. Details of the contacts made at the catalytic site for GPb–NFAG complex are shown in Figure 4B.

2.3. Comparison between NAG and NFAG binding

NFAG can be accommodated at the catalytic site, with essentially no disturbance of the structure. The superposition of the GPb–NFAG complex with the native T-state GPb over well-defined residues (18–249, 262–312 and 326–829) gave an r.m.s. deviation of 0.179 Å for Cα atoms, indicating that the two structures are overall similar. There are no changes at the allosteric effector, the new allosteric, and the inhibitor sites or the tower/tower subunit interface.

A structural comparison between the GPb–NAG complex and the GPb–NFAG complex shows that the two proteins also have very similar overall structures (Fig. 5); the structures superimpose quite well and they resemble each other in the vicinity of the catalytic site; the positions of the Ca, main-chain and side-chain atoms for residues 18–249, 262–312 and 326–829 deviate from their mean positions by 0.072, 0.094 and 0.465 Å, respectively, indicating overall negligible changes between the complex structures. However, comparison reveals an interesting conformational shift for residue Asp339. In the GPb–NFAG complex (as compared with the GPb–NAG complex), the CA, CB and CG of Asp339 are shifted by 0.3, 0.45 and 0.7 Å, respectively. The dihedral angle χ^2 [CA-CB-CG-OD1] is rotated by

Table 2. Hydrogen bond interactions between NAG, NFAG and residues at the catalytic site of GPb

Inhibitor atom	GPb–NAG		GPb–NFAG	
	Protein atom	Distance (Å)	Protein atom	Distance (Å)
N1	His377 O	2.9	His377 O	2.8
O2	Asn284 ND2	3.1	Asn284 ND2	3.0
	Tyr573 OH	3.3	Tyr573 OH	3.1
	Glu672 OE1	3.3	Glu672 OE1	3.2
	Wat258	2.7	Wat254	2.8
	Wat314	(3.4)	Wat319	3.3
O3	Glu672 OE1	2.7	Glu672 OE1	2.7
	Ser674 N	3.2	Ser674 N	3.1
	Gly675 N	3.1	Gly675 N	3.2
O4	Gly675 N	2.9	Gly675 N	2.9
	Wat200	2.5	Wat196	2.6
O6	His377 ND1	2.6	His377 ND1	2.7
	Asn484 OD1	2.8	Asn484 OD1	2.8
O7	Wat105	2.5	Wat100	2.8
	Wat355	3.0	Wat315	3.1
(F2			Wat315	3.2)
(F3			Wat315	3.2)

Water-mediated interactions. NAG: Wat258 is hydrogen bonded to Ala673 N, Thr671 O, and to Thr671 O, Val379 N and Wat256 through Wat257; Wat200 is hydrogen bonded to Thr676 N, OG1 and PLP O3P; Wat105 is hydrogen bonded to Leu136 N, Asp283 OD1, and to Leu136 N, Gly137 N, Gly134 N and Glu88 OE2 through Wat199; Wat355 is hydrogen bonded to Asn284 N and to Asn133 ND2, Glu88 OE1 and Asn282 O through Wat106. NFAG: Wat245 is hydrogen bonded to Ala673 N, Thr671 O and to Thr671 O, Val379 N and Wat252 through Wat253; Wat196 is hydrogen bonded to Thr676 N, OG1 and PLP O3P; Wat100 is hydrogen bonded to Leu136 N, Asp283 OD1 and to Leu136 N, Gly137 N, Gly134 N and Glu88 OE2 through Wat195; Wat315 is hydrogen bonded to Asn284 N, and to Asn133 ND2, Glu88 OE1 and Asn282 O, and Asn284 N, Phe285 N and Wat103 through Wat101 and Wat314, respectively.

91° to avoid close contacts with the fluorine atoms of NFAG. In its new position, the carboxyl group of Asp339 is hydrogen bonded to His377 N. Following the conformational change of Asp339, Wat318 also shifts by ~1.1 Å to maintain its hydrogen bond with Asp339 OD1. Furthermore, Wat315 shifts away (0.4 Å) from the ligand to create more space for the trifluoroacetyl group to be accommodated without causing steric hindrance.

3. Discussion

Bioisosters have been used to improve the properties of a molecule and obtain new classes of compounds.[31–33] Substitution of a hydrogen by fluorine is one of the most common methods of bioisosteric changes employed by medicinal chemists, possibly endowing enhanced pharmacological activity,[34,35] novel electrostatic interactions to the modified analogue, such as hydrogen bonding, and favourable van der Waals interactions with protein residues at the catalytic site of an enzyme.[36,37]

This study provides high-resolution structures of GPb in complex with two bioisosteric molecules, NAG and NFAG. The NFAG analogue binds with a 2.3-fold decreased affinity, relative to the corresponding unfluorinated analogue. The result is reminiscent of that of the binding of D-Ala ($K_d \approx 3.0 \pm 0.8$ mM) and D-F_3-Ala ($K_d = 6.2 \pm 0.6$ mM) to *Rhodotorula gracilis* D-amino acid oxidase.[38] Comparison of the NAG and NFAG complexes revealed that the most significant differences between the two structures are shifts of Asp339, and two water molecules on binding NFAG, which are absent in the interaction with NAG. In fact, being larger than hydrogen, the fluorine atom can cause unfavourable steric interactions with Asp339 and water structure in the catalytic site; the terminal $-CF_3$ does come close to the side chain of Asp339, but the carboxylate group rotates 90° about the CB-CG bond to avoid contact with the inhibitor.

The decrease in binding energy associated with trifluorosubstitution of the acetyl group of NAG is however contradictory with respect to the increase in the number of van der Waals contacts. It is possible that, in the GPb–NFAG complex, the energy gain due to the additional van der Waals interactions is outbalanced by the energy loss due to the conformational change of Asp339 and the bulkier fluorine atoms—since the fluorine atom has a van der Waals radius of 1.35 Å compared to hydrogen with a radius of 1.2 Å, leading to a lower binding affinity ($K_i = 75$ μM) compared to NAG ($K_i = 32$ μM). However, it cannot be excluded that other factors are involved in the reduced binding energy for NFAG, including increased hydrophilicity. It has been reported that fluorine can also form hydrogen bonds with water, which could influence its partitioning between freely solvated and enzyme-bound states.[39] On the other hand, hydrophilicity of the trifluoromethyl group may differ according to the carbon skeleton to which it is attached. For fluorinated aliphatic carbonyl compounds, the apparent hydrophilicity depends even on the choice of partitioning solvents.[40,41] Unfortunately, we were unable to locate relevant literature data for the hydrophilicities of acetamide- and trifluoroacetamide-type compounds, except for one report on 4-nitrophenyl 2-acylamido-2-deoxy-β-D-glucosaminides.[42] In this paper, a considerably higher hydrophilicity is invoked for the trifluoroacetamide than the acetamide derivative, which can be similar for NFAG and NAG, respectively.

4. Materials and methods

The synthesis of NFAG (Scheme 1) was described previously.[20] NAG was kindly provided by Prof. G. W. J. Fleet. Rabbit GPb was isolated, purified, recrystallised and assayed as described.[17] Kinetic experiments were performed in the direction of glycogen synthesis in the presence of constant concentrations of glycogen (1% w/v), AMP (1 mM) and various concentrations of Glc-1-P (1.5–20 mM) and inhibitor (44–178 μM). The inorganic phosphate released in the reaction was determined as previously.[44]

Native T-state GPb crystals, grown in the tetragonal lattice,[45] space group $P4_32_12$, were soaked with 10 mM NAG (for 1 h) or 100 mM NFAG (for 30 min) in a buffered solution (10 mM Bes, 0.1 mM EDTA and 0.02%

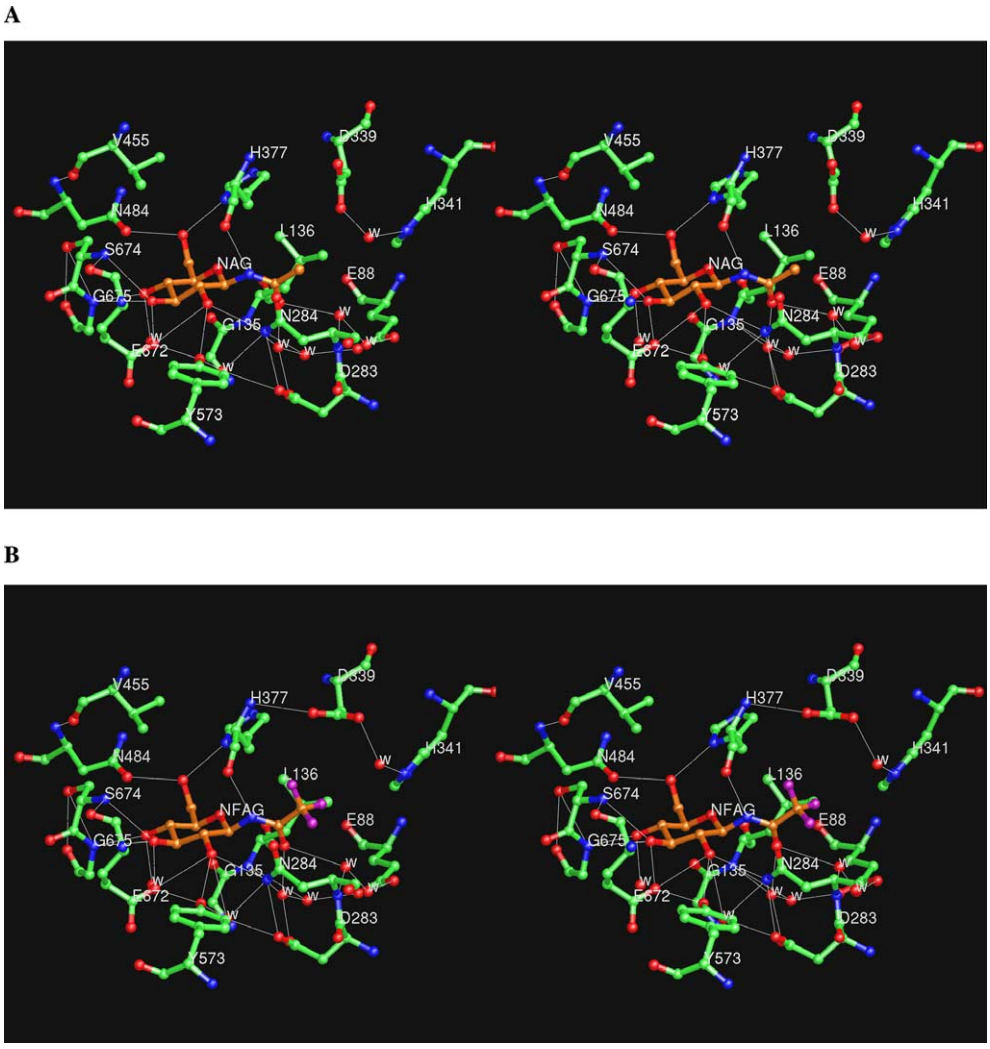

Figure 4. Stereo diagrams showing interactions between NAG (A) and NFAG (B) and protein in the vicinity of the catalytic site.

sodium azide, pH 6.7), prior to data collection. Data for the GPb–NFAG complex were collected from a single crystal on Station 9.6 at Daresbury Laboratory to 1.8 Å resolution ($\lambda = 0.87$ Å). Data for the GPb–NAG complex were collected at ESRF, Grenoble, by translating a single crystal and successively exposing small sections to the beam ($\lambda = 0.933$ Å), at a resolution of 1.9 Å. The reflections were recorded on an ADSC Q4 CCD detector for both complexes. Data reduction and integration, followed by scaling and merging of the intensities obtained, were performed with Denzo and Scalepack, respectively, as implemented in a HKL suite.[46]

Crystallographic refinement of both complexes was performed with CNS version 1.1[47] using positional and individual B-factor refinement with bulk-solvent correction. The starting model employed for the refinement of both complexes was the structure of GPb–NAG–IMP complex determined at 2.3 Å resolution.[17] For both data sets, there was sufficient ($2F_o - F_c$) and ($F_o - F_c$) electron density to accommodate the ligands at the catalytic site. The NFAG model was built using the program QUANTA (QUANTA Version 3.3, 1992, Molecular Simulations, Inc., 200 Fifth Avenue Waltham, MA 02154), where the hydrogen atoms of the methyl group of C8 of NAG were replaced by fluorine atoms. Alternate cycles of manual rebuilding with the program 'O'[48] and refinement with CNS improved the quality of the models. The stereochemistry of the protein residues was validated by PROCHECK.[49,50] Hydrogen bonds and van der Waals interactions were calculated with the program CONTACT, as implemented in CCP4[50] applying a distance cut-off of 3.3 and 4.0 Å, respectively. The program calculates the angle O...H...N (where the position of hydrogen is unambiguous) and the angle source ...oxygen-bonded carbon atom. Suitable values are 120° and 90°. The Luzatti plots[30] suggest an average positional error for both structures of approximately 0.21 Å. The protein structures were superimposed using LSQKAB.[50] The schematic representation of the crystal structures presented in all figures were prepared with the program XOBJECTS (M. E. M. Noble, unpublished results). The coordinates of the new structures have been deposited with the RCSB Protein Data Bank (http://www.rcsb.org/pdb), with codes 1WW2 (GPb–NAG complex) and 1WW3 (GPb–NFAG complex).

Table 3. van der Waals interactions between compounds NAG, NFAG and residues at the catalytic site of GPb

Inhibitor atom	GPb–NAG		GPb–NFAG	
	Protein atom	No. of contacts	Protein atom	No. of contacts
C1	His377 O	1	His377 O	1
N	Asn284 OD1, ND2; His377 C, CB	4	Asn284 ND2; His377 C, CB	3
C2	His377 O; Glu672 OE1; Ala673 CB; Wat258	4	His377 O; Glu672 OE1; Wat254	3
O2	Asn284 CG, OD1; His377 O	3	Asn284 CG, OD1; His377 O	3
C3	Glu672 OE1; Gly675 N; Wat200	3	Glu672 OE1; Gly675 N; Wat196	3
O3	Glu672 CG, CD; Ala673 N; Ser674 C, CA; Gly675 CA	6	Glu672 C, CG, CD; Ala673 N, C, CA, CB; Ser674 CA; Gly675 CA; Wat254	10
C4	Gly675 N; Wat200	2	Gly675 N; Wat196	2
O4	Asn484 OD1; Ser674 C, CB; Gly675 C, CA, O; Thr676 CG2	7	Asn484 OD1; Ser674 C, CB; Gly675 C, CA, O	6
C5	Gly135 C; Leu136 N; Wat200	3	Gly135 C; Leu136 N; Wat196	3
O5	His377 CB, CG, O, ND1	4	His377 CB, O, ND1	3
C6	Gly135 C, O; Leu139 CD2; His377 ND1; Asn484 OD1	5	Gly135 C, O; Leu136 CA; His377 ND1; Asn484 OD1	5
O6	Leu139 CD2; His377 CG, CE1; Val455 CG1; Asn484 CG	5	Leu139 CD2; His377 CG, CE1; Val455 CG1, CG2; Asn484 CG	6
C7	Asn284 CG, OD1, ND2; Wat105; Wat355	5	Asn284 ND2; His377 CB, O; Wat315	4
O7	Leu136 CB, CD2; Asn284 ND2	3	Leu136 CB; Asn284 ND2	2
C8	Asn284 CG, OD1, ND2; Asp339 OD1; Wat110; Wat355	6	Asn284 OD1; Wat315	2
F1			Asp339 OD2; His377 C, CA, CB, O; Thr378 N, CB, CG2	8
F2			Asn284 N, CA, CB, CG, ND2, OD1; Thr378 CG2, Wat314	8
F3			Leu136 CD2; Wat314; Wat318	3
	Total	61		75

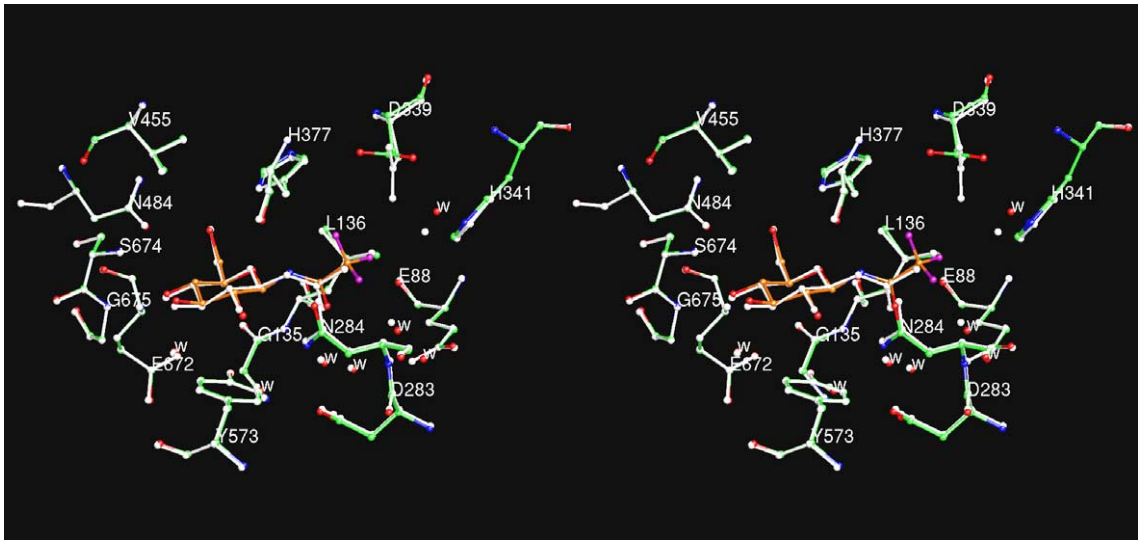

Figure 5. Stereo diagram of the superimposed structures of NAG complex (white) onto the NFAG complex (green) in the vicinity of the catalytic site.

Acknowledgments

This work was supported by Greek GSRT through PE-NED-204/2001 (MNK), and ENTER-EP6/2001 (EDC), the Hungarian Scientific Research Fund (OTKA T43550 to Z. Gy.) the Joint Research and Technology project between Greece and Hungary (2005–2006) (to N.G.O and L.S.), SRS Daresbury Laboratory (contract IHPP HPRI-CT-1999-00012) and ESRF (contract HPRI-CT-1999-00022). We also wish to acknowledge the assistance of Ms. Rozina Kardakaris and Dr. Vicky Skamnaki for help in kinetics and data collection.

References and notes

1. Aiston, S.; Hampson, L.; Gómez-Foix, A. M.; Guinovart, J. J.; Agius, L. *J. Biol. Chem.* **2001**, *276*, 23858.
2. McCormack, J. C.; Westergaard, N.; Kristiansen, M.; Brand, C. L.; Lau, J. *Curr. Pharm. Des.* **2001**, *7*, 1451.
3. Treadway, J. L.; Mendys, P.; Hoover, D. J. *Expert Opin. Investig. Drugs* **2001**, *10*, 439.
4. Latsis, T.; Andersen, B.; Agius, L. *Biochem. J.* **2002**, *368*, 309.
5. Aiston, S.; Coghlan, M. P.; Agius, L. *Eur. J. Biochem.* **2003**, *270*, 2773.
6. Oikonomakos, N. G. *Curr. Protein Pept. Sci.* **2002**, *3*, 561.
7. Kurukulasuriya, R.; Link, J. T.; Madar, D. J.; Pei, Z.; Richards, S. J.; Rohde, J. J.; Souers, A. J.; Szczepankiewicz, B. G. *Curr. Med. Chem.* **2003**, *10*, 123.
8. Lu, Z.; Bohn, J.; Bergeron, R.; Deng, Q.; Ellsworth, K. P.; Geissler, W. M.; Harris, G.; McCann, P. E.; McKeever, B.; Myers, R. W.; Saperstein, R.; Willoughby, C. A.; Yao, J.; Chapman, K. *Bioorg. Med. Chem. Lett.* **2003**, *13*, 4125.
9. Ogawa, A. K.; Willoughby, C. A.; Bergeron, R.; Ellsworth, K. P.; Geissler, W. M.; Myers, R. W.; Yao, J.; Harris, G.; Chapman, K. T. *Bioorg. Med. Chem. Lett.* **2003**, *13*, 3405.
10. Somsák, L.; Nagy, V.; Hadady, Z.; Docsa, T.; Gergely, P. *Curr. Pharm. Des.* **2003**, *9*, 1177.
11. Kristiansen, M.; Andersen, B.; Iversen, L. F.; Westergaard, N. *J. Med. Chem.* **2004**, *47*, 3537.
12. Wright, S. W.; Rath, V. L.; Genereux, P. E.; Hageman, D. L.; Levy, C. B.; McLure, L. D.; McCoid, S. C.; McPherson, R. K.; Schelhorn, T. M.; Wilder, D. E.; Zavadoski, W. J.; Gibbs, E. M.; Treadway, J. L. *Bioorg. Med. Chem. Lett.* **2005**, *15*, 459.
13. Somsák, L.; Nagy, V.; Hadady, Z.; Felföldi, N.; Docsa, T.; Gergely, P. In *Frontiers in Medicinal Chemistry*; Reitz, A. B., Kordik, C. P., Choudhary, M. I., Atta-ur-Rahman, Eds.; Bentham, 2005; Vol. 2, pp 253–272.
14. Martin, J. L.; Veluraja, K.; Johnson, L. N.; Fleet, G. W. J.; Ramsden, N. G.; Bruce, I.; Oikonomakos, N. G.; Papageorgiou, A. C.; Leonidas, D. D.; Tsitoura, H. S. *Biochemistry* **1991**, *30*, 10101.
15. Watson, K. A.; Mitchell, E. P.; Johnson, L. N.; Son, J. C.; Bichard, C. J. F.; Orchard, M. G.; Fleet, G. W. J.; Oikonomakos, N. G.; Leonidas, D. D.; Kontou, M.; Papageorgiou, A. C. *Biochemistry* **1994**, *33*, 5745.
16. Bichard, C. J. F.; Mitchell, E. P.; Wormald, M. R.; Watson, K. A.; Johnson, L. N.; Zographos, S. E.; Koutra, D. D.; Oikonomakos, N. G.; Fleet, G. W. J. *Tetrahedron Lett.* **1995**, *36*, 2145.
17. Oikonomakos, N. G.; Kontou, M.; Zographos, S. E.; Watson, K. A.; Johnson, L. N.; Bichard, C. J. F.; Fleet, G. W. J.; Acharya, K. R. *Protein Sci.* **1995**, *4*, 2469.
18. Watson, K. A.; Mitchell, E. P.; Johnson, L. N.; Cruciani, G.; Son, J. C.; Bichard, C. J. F.; Fleet, G. W. J.; Oikonomakos, N. G.; Kontou, M.; Zographos, S. E. *Acta. Crystallogr. D* **1995**, *51*, 458.
19. Gregoriou, M.; Noble, M. E. M.; Watson, K. A.; Garman, E. F.; Krulle, T. M.; Fuente, C.; Fleet, G. W. J.; Oikonomakos, N. G.; Johnson, L. N. *Protein Sci.* **1998**, *7*, 915.
20. Somsák, L.; Kovács, L.; Tóth, M.; Ösz, E.; Szilágyi, L.; Györgydeák, Z.; Dinya, Z.; Docsa, T.; Tóth, B.; Gergely, P. *J. Med. Chem.* **2001**, *44*, 2843.
21. Oikonomakos, N. G.; Skamnaki, V. T.; Ösz, E.; Szilágyi, L.; Somsák, L.; Docsa, T.; Tóth, B.; Gergely, P. *Bioorg. Med. Chem.* **2002**, *10*, 261.
22. Oikonomakos, N. G.; Kosmopoulou, M.; Zographos, S. E.; Leonidas, D. D.; Chrysina, E. D.; Somsák, L.; Nagy, V.; Praly, J.-P.; Docsa, T.; Tóth, B.; Gergely, P. *Eur. J. Biochem.* **2002**, *269*, 1684.
23. Chrysina, E. D.; Oikonomakos, N. G.; Zographos, S. E.; Kosmopoulou, M. N.; Bischler, N.; Leonidas, D. D.; Kovács, L.; Docsa, T.; Gergely, P.; Somsák, L. *Biocatal. Biotransform.* **2003**, *21*, 233.
24. Györgydeák, Z.; Hadady, Z.; Felföldi, N.; Krakomperger, A.; Nagy, V.; Tóth, M.; Brunyánszki, A.; Docsa, T.; Gergely, P.; Somsák, L. *Bioorg. Med. Chem.* **2004**, *12*, 4861.
25. Chrysina, E. D.; Kosmopoulou, M. N.; Kardakaris, R.; Bischler, N.; Leonidas, D. D.; Kannan, T.; Loganathan, D.; Oikonomakos, N. G. *Bioorg. Med. Chem.* **2005**, *13*, 765.
26. Chrysina, E. D.; Kosmopoulou, M. N.; Tiraidis, C.; Kardakaris, R.; Bischler, N.; Leonidas, D. D.; Hadady, Z.; Somsák, L.; Docsa, T.; Gergely, P.; Oikonomakos, N. G. *Protein Sci.* **2005**, *14*, 273.
27. Board, M.; Hadwen, M.; Johnson, L. N. *Eur. J. Biochem.* **1995**, *228*, 753.
28. Board, M.; Bollen, M.; Stalmans, W.; Kim, Y.; Fleet, G. W. J.; Johnson, L. N. *Biochem. J.* **1995**, *311*, 845.
29. Board, M.; Johnson, L. N. *Diabetes Res.* **1995**, *28*, 95.
30. Luzatti, V. *Acta Crystallogr.* **1952**, *5*, 802.
31. Burger, A. *Prog. Drug Res.* **1991**, *37*, 287.
32. Papani, G. A.; LaVoie, E. J. *Chem. Rev.* **1996**, *96*, 3147.
33. Olesen, P. H. *Curr. Opin. Drug Discov. Devel.* **2001**, *4*, 471.
34. Resnati, G. *Farmaco* **1990**, *45*, 1043.
35. Bryskier, A.; Chantot, J. F. *Drugs* **1995**, *49*, 16.
36. Chong, Y.; Choo, H.; Chu, C. K. *Bioorg. Med. Chem. Lett.* **2004**, *14*, 437.
37. Lindberg, J.; Pyring, D.; Löwgren, S.; Rosenquist, Å; Zuccarello, G.; Kvarnström, I.; Zhang, H.; Vrang, L.; Classon, B.; Hallberg, A.; Samuelsson, B.; Unge, T. *Eur. J. Biochem.* **2004**, *271*, 4594.
38. Umhau, S.; Pollegioni, L.; Molla, G.; Diederichs, K.; Welte, W.; Pilone, M. S.; Ghisla, S. *Proc. Natl. Acad. Sci. U.S.A.* **2000**, *97*, 12463.
39. Schwartz, B.; Drueckhammer, D. G.; Usher, K. C.; Remington, S. J. *Biochemistry* **1995**, *34*, 15459.
40. Welch, J. *Tetrahedron* **1987**, *43*, 3123.
41. Organofluorine Chemistry. Principles and Commercial Applications, Banks, R. E., Smart, B. E., Tatlow, J. C., Eds.; Plenum Press, New York and London, 1994.
42. Yamamoto, K. *J. Biochem.* **1974**, *76*, 385.
43. Leatherbarrow, R. J. *Trends Biochem. Sci.* **1990**, *15*, 455.
44. Saheki, S.; Takeda, A.; Shimazu, T. *Anal. Biochem.* **1985**, *148*, 277–281.
45. Oikonomakos, N. G.; Melpidou, A. E.; Johnson, L. N. *Biochim. Biophys. Acta* **1985**, *832*, 248.
46. Otwinowski, Z.; Minor, W. *Methods Enzymol.* **1997**, *276*, 307.
47. Brünger, A. T.; Adams, P. D.; Clore, G. M.; DeLano, W. L.; Gros, P.; Grosse-Kunstleve, R. W.; Jiang, J.-S.; Kuszewski, J.; Nilges, M.; Pannu, N. S.; Read, R. J.; Rice, L. M.; Simonson, T.; Warren, G. L. *Acta. Crystallogr. D* **1998**, *54*, 905.
48. Jones, T. A.; Zou, J. Y.; Cowan, S. W.; Kjeldgaard, M. *Acta. Crystallogr. A* **1991**, *47*, 110.
49. Laskowski, R. A.; MacArthur, M. W.; Moss, D. S.; Thornton, J. M. *J. Appl. Crystallogr.* **1993**, *26*, 283.
50. Collaborative Computational Project No 4. *Acta Crystallogr. D* **1994**, *50*, 760.